water

MDPI

*Article*

# Heterogeneous Fenton-like Photocatalytic Process towards the Eradication of Tetracycline under UV Irradiation: Mechanism Elucidation and Environmental Risk Analysis

**Mohamadamin Amarzadeh [1,†], Moslem Azqandi [2,†], Kasra Nateq [3], Bahman Ramavandi [4], Nadeem A. Khan [5,*] and Negin Nasseh [6,7,*]**

1 Department of Safety Engineering, Abadan Faculty of Petroleum Engineering, Petroleum University of Technology, Abadan 6318714317, Iran
2 Student Research Committee, Birjand University of Medical Sciences, Birjand 9717853076, Iran
3 Department of Chemical Engineering, Abadan Faculty of Petroleum Engineering, Petroleum University of Technology, Abadan 6318714317, Iran
4 Environmental Health Engineering Department, Faculty of Health and Nutrition, Bushehr University of Medical Sciences, Bushehr 7514633196, Iran
5 Interdisciplinary Research Center for Membranes and Water Security, King Fahd University of Petroleum and Minerals, Dhahran 31261, Saudi Arabia
6 Cellular and Molecular Research Center, Birjand University of Medical Sciences, Birjand 9717853076, Iran
7 Department of Health Promotion and Education, School of Health, Birjand University of Medical Sciences, Birjand 9717853076, Iran
* Correspondence: nadeem.khan@kfupm.edu.sa(N.A.K.); negin.nasseh2020@gmail.com (N.N.)
† These authors contributed equally to this work.

**Abstract:** The problem of the deep elimination of antibiotics in environmental bodies is exceptionally warranted. In this work, a ternary nanocomposite of $FeNi_3/SiO_2/CuS$ (FSC) was fabricated and then integrated with UV light irradiation and hydrogen peroxide as the heterogeneous Fenton-like photocatalytic system for the decomposition of tetracycline (TC) from aqueous media. During this process, various influencing parameters such as pH, catalyst dosage, initial content of TC, hydrogen peroxide ($H_2O_2$) dose, and operating time were explored. At optimized circumstances, i.e., 5 of pH, 10 mg/L of TC concentration, 150 mg/L of $H_2O_2$ dosage, and 200 min of degradation time, the elimination proportion of TC was 96%. The results of capture agent tests clarified that hydroxyl radical ($HO^{\bullet}$) played the predominant role in the photocatalytic decontamination of TC. Moreover, with the elevated contact time and content of $H_2O_2$, the efficiency of TC decontamination increased significantly. Additionally, the findings of the stability and reusability experiments of the fabricated nanocomposite showed that the percentage of TC removal decreased by only about 5% after six cycles. Furthermore, the photocatalytic mechanism of the decontamination of TC over the FSC photocatalyst was elucidated. Eventually, the non-carcinogenic risk analysis in the surface water sample was carried out using multiple photocatalytic processes for the first time. These outcomes obtained in this study validate that coupling the photocatalytic system and the $H_2O_2$ oxidation agent facilitates the elimination of a great variety of pharmaceutical contaminants from aqueous media.

**Keywords:** $FeNi_3/SiO_2/CuS$ magnetic nanocomposite; tetracycline; degradation; heterogeneous photocatalytic Fenton-like process

check for updates

**Citation:** Amarzadeh, M.; Azqandi, M.; Nateq, K.; Ramavandi, B.; Khan, N.A.; Nasseh, N. Heterogeneous Fenton-like Photocatalytic Process towards the Eradication of Tetracycline under UV Irradiation: Mechanism Elucidation and Environmental Risk Analysis. *Water* **2023**, *15*, 2336. https://doi.org/10.3390/w15132336

Academic Editor: Zacharias Frontistis

Received: 28 May 2023
Revised: 16 June 2023
Accepted: 20 June 2023
Published: 23 June 2023

**Copyright:** © 2023 by the authors. Licensee MDPI, Basel, Switzerland. This article is an open access article distributed under the terms and conditions of the Creative Commons Attribution (CC BY) license (https://creativecommons.org/licenses/by/4.0/).

## 1. Introduction

The increase in population, the expansion of urbanization, and the progress of industries are considerable matters that have resulted in the enhancement of environmental and ecological concerns in recent times [1]. Antibiotics, as antibacterial compounds, are an environmental problem due to their excessive use by humans in the fields of medicine, veterinary medicine, agriculture, aquaculture, etc. [2]. The annual consumption of antibiotics

is estimated between 100,000 and 200,000 t per year, which accounts for approximately 15% of all drugs used worldwide [3]. High toxicity, low biodegradability, and high solubility in water are notable drawbacks of antibiotics, which lead to their classification as emerging pollutants even at low concentrations [4,5]. The most widely used antibiotics can be divided into quinolones, tetracyclines (TCs), aminoglycosides, macrolides, and sulfonamides according to their chemical nature [6]. So far, many purification procedures have been conducted to remove TC, such as adsorption [7], electrocoagulation [8], advanced biological processes [9], activated persulfate processes [10,11], activated peracetic acid processes [12,13], ozonation [14], and membrane processes [15]. The implementation of these methods is considered inefficient for eliminating TC from aqueous solutions due to several substantial shortcomings, such as high energy consumption, incomplete TC decomposition, long-lasting treatment, and the formation of secondary pollutants [16,17]. The photocatalytic process based on semiconductors is a type of advanced oxidation process (AOPs) that has brought some advantages in eliminating organic pollutants, especially antibiotics owing to the high oxidation rate of pollutants, limited production of secondary pollutants, and low energy consumption [18]. The principal mechanism of the photocatalytic process is to irradiate light as an external energy source on the catalyst surface that results in the generation of holes ($hole^+$ or $h^+$) in the valence band (VB) and likewise the excitation of electrons ($e^-$ and transfer them to the conduction band (CB) [19]. During this process, the $h^+$ and $e^-$ agents are produced by the decomposition of water and oxygen molecules, causing the formation of hydroxyl ($HO^\bullet$) and superoxide ($O_2^{\bullet-}$) radicals. The mentioned oxidizing radicals have a high ability to degrade organic pollutants, such as TCs [20]. Recently, CuS nanoparticles with organic–metallic bonds and a 2 eV band gap have drawn a lot of attention to remove organic compounds from aqueous environments due to their non-toxicity, low cost, and suitable stability under ambient conditions [21]. However, the individual use of CuS nanoparticles is an inappropriate semiconductor candidate for the photocatalytic decomposition of refractory organic contaminants because of its difficulty in recovery and reusability, high consumption, blocking of the active surface, and weak absorption of light energy [21–23]. To circumvent these limitations, we designed integrating two oxidation procedures to increase the mineralization degree of the contaminant decomposition system. The first method is the photocatalytic process based on anchoring semiconductors on porous solid materials such as carbon [24], silica [25], clay [26], and magnetic core [27]. In this vein, the modification of the catalyst surface will be improved the performance of photocatalytic procedures owing to increasing the pollutant adsorption rate, reducing pollutant accumulation on the catalyst surface, enhancement of the catalyst recovery capacity, and suppressing the recombination rate of photoexcited electrons and holes [28]. The second method of the proposed integration degradation system includes the employment of a heterogeneous Fenton-like process. This procedure is an effective approach to degrading and mineralizing organic pollutants because of its simplicity, relatively cost-effective destruction system, and high production of $HO^\bullet$ radicals [29]. The reaction of Fenton-like processes is formed to destroy stubborn pollutants by activating hydrogen peroxide ($H_2O_2$) as a strong oxidant and iron ions as a catalyst. Nonetheless, the Fenton-like process has faced several crucial drawbacks, such as forming large amounts of sludge containing iron oxides, sufficient degradation performance only in the range of acidic pH, and requiring high concentration of iron ions, which have led to the implementation of them to be inappropriate in environmental remediation issues [30]. Therefore, due to these restrictions of Fenton-like processes, the heterogeneous Fenton procedures have been increasingly implemented for eliminating contaminants in recent studies, such as iron and metallic-based materials [29]. $FeNi_3$ is one of the iron-based materials, which has been an excellent candidate for application as a catalyst in the heterogeneous Fenton process because of its facile fabrication, high permeability, ease of separation and recovery, and high destruction performance of organic contaminants [31]. However, several weaknesses have been reported in the utilization of the $FeNi_3$ nanoparticle in AOPs, such as low adsorption of pollutants, improper energy losses, instability, accumulation and sedimentation

in environmental waters, and high temperature [32]. Up to now, numerous studies have been presented modifying the surface of the nanoparticles with metal oxide materials for ameliorating the negative properties of $FeNi_3$ [33]. The $SiO_2$ nanoparticle is one of the metal oxide materials, which can be functionalized with $FeNi_3$ to effectively enhance its features, for instance, improving the electrical resistance and prevention of oxidizing the catalyst [34]. Moreover, the $FeNi_3$ coated with $SiO_2$ results in the enhancement of the heterogeneous-Fenton-like photocatalytic system through decomposing more $H_2O_2$ to $HO^{\bullet}$ radicals [35].

Multiple works have been conducted using $FeNi_3$, CuS, and $SiO_2$ for the photo-decontamination of pharmaceutical substance-laden wastewater so far, which in some cases are similar to the present study. Alwared et al., (2022) scrutinized the decontamination efficiency of amoxicillin utilizing $FeNi_3@SiO_2@TiO_2$ (FST) as a photocatalyst in a batch system. The findings indicated that the FST material offers excellent photocatalytic ability for efficient and environmentally-friendly decomposition of amoxicillin [36]. Kamranifar et al., (2021) comprehensively evaluated the photo-decontamination performance of $FeNi_3@SiO_2@ZnO$ for penicillin G (PNG) elimination and achieved a PNG degradation rate of 100% [37]. Nonetheless, the objective of the current study is more comprehensive rather than similar studies. In the present work, the catalytic performance of the $FeNi_3/SiO_2/CuS$ (FSC) material was scrutinized for the decontamination of TC deploying the heterogeneous Fenton-like photocatalytic procedure under UV illumination and $H_2O_2$. The impact of radical quenchers, kinetic studies, and nanocomposite reusability were also examined in detail. Finally, as the foremost notable part and innovation of the current study, the health risks of TC-contained actual water source after the purification were assessed after implementing the $FeNi_3/SiO_2/CuS/UV/H_2O_2$ system.

## 2. Experimental Section

### *2.1. Materials and Reagents*

To synthesize the target material, the following chemicals were utilized: divalent iron chloride ($FeCl_2{\cdot}4H_2O$), polyethylene glycol (PEG 6000), nickel chloride ($NiCl_2.6H_2O$) ethylene glycol ($C_2H_6O_2$), tetra Ethyl orthosilicate (TEOS), hydrazinium hydrate ($N_2H_4{\cdot}H_2O$), copper sulfate ($CuSO_4$), ammonia ($NH_3$), and sodium thiosulfate ($Na_2S_2O_3$). The analytical grade of all the aforementioned chemicals was manufactured by Merck Company (Munich, Germany). In addition, TC powder ($C_{22}H_{24}N_2O_8$, >95%) was procured from Sigma-Aldrich (Munich, Germany). Whole solutions were provided with deionized water.

### *2.2. Reactor Specifications*

To provide a UV illumination source, a UV lamp 18W (PHILIP Co., Ltd., Pekan, Japan), and highest emission at a wavelength of 254 nm was utilized. The lamp was located inside a quartz sheath in the middle of the steel-designed reactor. The UV radiation intensity was 2500 mW/($cm^2$). A cooling water wall placed around the quartz sheath was utilized to keep the reactor temperature in the span of 24 ± 2 °C. Samples were taken from the suspension at specified removal time intervals. Then, the remaining TC content was quantified through a UV-vis spectrophotometer.

### *2.3. Synthesis of the Constructed Magnetic Nanocomposite*

First, $FeNi_3/SiO_2$ (FS) material was synthesized based on previous studies [38]. Subsequently, $FeNi_3/SiO_2$ (0.15 g) was added to 20 mL EG and dispersed for 30 min in an ultrasonic device. Then, the prepared material was transferred to a 500 mL flask and situated in an oil bath at 120 °C. In the following step, 0.8 g $CuSO_4$ was added to the achieved suspension and continuously dissolved under the sonication process to obtain the homogeneous suspension. Next, 1.9 g $Na_2S_2O_3$ was poured into the prepared mixture, then continuously heated at 140 °C for 90 min. In the end, the fabricated magnetic nanocomposite (FSC) was collected by a magnetic magnet and rinsed multiple times with ethanol and deionized water, and subsequently was dried in a drying oven at 80 °C for 5 h.

### *2.4. TC Degradation Experiments Utilizing the $FeNi_3/SiO_2/CuS/UV/H_2O_2$ System*

The TC photodecomposition tests were carried out in a batch system and ambient temperature (20 ± 2 °C) utilizing TC solution (200 mL) under UV illumination. Each stage of the experiment was repeated three times. The influence of affecting variables, including the level of initial pH (3–11), the nanocomposite quantity (0.005–0.1 g/L), initial TC content (10–30 mg/L), operating time (5–200 min), and quantity of $H_2O_2$ (50–200 mg/L) were examined in this work. The pH level of the solution was adjusted using HCl (1M) and NaOH (1M) under extreme stirring (the speed of 350 rpm). The samples were taken at certain intervals, and the residual content of TC was determined through a UV-vis spectrophotometer. The rate of TC decontamination was computed based on Equation (1) [39].

$$R(\%) = [(TC_0 - TC_t\ )/TC_0] \times 100 \quad (1)$$

where $TC_0$ (mg/L) and $TC_t$ (mg/L) are the initial concentration and remaining content of TC, respectively. R (%) is equal to the proportion of TC elimination.

The total organic carbon (TOC) findings were quantified using a TOC analyzer (Shimadzu Co., Ltd., Pekan, Japan). Radical scavenging tests were employed to determine the contributing species responsible for the photocatalytic process. The quenchers included isopropanol (IPA, 20 mM) for hydroxyl radical ($HO^{\bullet}$), ethylenediaminetetraacetic acid (EDTA, 20 mM) for photogenerated holes ($h^+$), chloroform (20 mM) for the superoxide radical ($O_2^{\bullet -}$), and potassium persulfate ($K_2S_2O_8$, 30 mM) for $e^-$.

### *2.5. Photo-Decontamination Kinetics*

Generally, the rate of heterogeneous catalytic reactions is examined by the pseudo-first-order kinetic model. This study scrutinized the kinetics of photo-decontamination of TC over the $FeNi_3/SiO_2/CuS/UV/H_2O_2$ system adopting the Langmuir–Hinshelwood (L-H) kinetic model, as illustrated by Equation (2) [40].

$$r = k'\theta = -\frac{d_c}{d_t} = k/(\frac{kc}{1+kc}) \quad (2)$$

where r (mg/L min) = initial reaction rate, k = reaction rate constant, C (mg/L) = contaminant content, k′ = adsorption coefficient, and θ = reaction site. For solutions with very low contents (such as antibiotics in water media) with k << 1, the L-H equation (Equation (2)) can be converted to as follows (Equations (3) and (4)):

$$-\frac{dC}{dt} = k_{obs}C \quad (3)$$

$$\ln\left(\frac{C}{C_0}\right) = -k_{obs}t \quad (4)$$

In this equation, $k_{obs}$ (1/min) is the rate constant of the pseudo-first-order model, t (min)= reaction time, C (mg/L) is the remaining TC content, and $C_0$ (mg/L) = initial concentration of the TC.

### *2.6. Regeneration Experiment of the Constructed Nanocomposite*

The performance of materials is evaluated in terms of regeneration tests to investigate their cost-effectiveness and stability [41]. For this purpose, in the current work, the ability of FSC was examined for TC decontamination through six consecutive cycles under optimized operating conditions (20 mg/L of TC concentration, 0.005 g/L of catalyst dose, 200 min of oxidation time, 5 of pH, and 150 mg/L of $H_2O_2$ content). The FSC nanocomposite was magnetically separated from the solution after each run. Then, the sample was washed several times with deionized water and finally dried at 80 °C. The reusability of the nanocomposite was investigated in up to 6 steps.

### 2.7. Evolution of Human Health Risk

The human risk of TC contaminating the real water source was accomplished through the software of Oracle® Crystal Ball (version 11.1.2.3). Firstly, the application of various photocatalytic methods for eliminating TC from the mentioned real water sample was conducted at optimized operational factors, in which the initial concentration of TC was measured to be 7.5 ng/L. Subsequently, the value of chronic daily intake (CDI) and the hazard quotient (HQ) of TC was computed utilizing the mentioned oxidation processes based on Equations (5) and (6), respectively.

$$\mathrm{CDI} = \frac{\mathrm{C} \times \mathrm{CF} \times \mathrm{CR} \times \mathrm{CD}}{(\mathrm{BW} \times \mathrm{AT})} \quad (5)$$

$$\mathrm{HQ} = \frac{\mathrm{CDI}}{\mathrm{ADI}} \quad (6)$$

In the abovementioned equations, CDI is the rate of chronic daily consumption (μg/kg day), C is the concentration of TC (μg/L), CR is the amount of water consumption (2 L/day), CD is the period of water usage (70 years), BW is the weight of the body (71 kg), AT is the mean value of lifetime (25,550 days), CF is the factor of conversion (365 days/yr), and ADI is the permissible daily intake (9.5 μg kg/day) [42].

## 3. Results and Discussion

### 3.1. Characterization Findings

The FESEM, EDX, FTIR, TGA, and VSM images of the FSC magnetic nanocomposite were exhibited in the previous studies [37–43]. The surface morphology of the synthesized nanocatalyst was found to be core–shell–shell according to FESEM analyses. The particle dimension of the nanocomposite is in the span of 26–64 nm, revealing the micrography of the nanocomposite is magnetic. Furthermore, it is observed that the material has a mass property and agglomeration tendency. This state of self-aggregation can be occurred because of its magnetic property, in which multiple particles of the composite attract each other or are replaced alongside each other. Moreover, the EDX test of the synthesized magnetic nanocomposite confirmed that each component of the target composite is present in the structure of the FSC composite. To complement the characterization of the magnetic nanocomposite, the TEM analysis was conducted, evidencing that its structure is amorphous and irregular with the high density of the composite. In addition, the FTIR graph of FSC composite represents that the absorption peak appeared at 440.2 $cm^{-1}$, revealing a sulfur heteroatom vibration with metal bonds, which the Cu-S bond is the foremost possible bond. The metallic bonds (Fe-Ni-Ni, Ni-Fe-Ni, and Fe-Ni) are related to the absorption peak detected at 636.96 $cm^{-1}$. The adsorption peak observed at near 887.8 $cm^{-1}$, corresponding to vibrating the bonds of Fe-Ni-Cu, Fe-Cu, and Ni-Cu. In addition, the adsorption peak at around 1016.6–1141.0 $cm^{-1}$ is attributed to the vibrative bonds of Ni-Fe-$SiO_2$, Fe-$SiO_2$, and Si-O. The peak in the wavenumber of 1609.5 $cm^{-1}$ corresponds to C-O or C-N, or C-H bonds, possibly owing to the occurrence of impurity substances stemming from hydrazine raw materials and polyethylene glycol.

According to the TGA patterns of the as-prepared composite, it is clearly observed that the weight loss alterations happened in the temperature ranging from 110 °C to 125 °C. During the temperature range, an endothermic procedure was come up due to the negative changes at the predetermined temperature period, causing water molecules and volatile matter (e.g., hydrazine hydrate) to be evaporated and released from the specimen. The evaporation of solvents led to a weight loss of approximately 0.92%. Then, 0.38% weight of the sample was lost at the temperature of 210 °C. It was ascribed to the evaporation of several impurity compounds absorbed through the surface of the catalyst over the synthesis procedure. Roughly the weight loss of the FSC composite was attained to be 0.52% over 650 °C owing to the endothermic process. The temperature is considered as the glass temperature or the transition glass temperature, indicating phase vibrations in the specimen.

The magnetic behavior of the nanocomposite was studied using a vibrating sample magnetometer (VSM) at room temperature. The FSC magnetic nanocomposite has a magnetization saturation value of 18.42 emu/g. The findings exhibited that the fabricated FSC nanocomposite could be rapidly magnetized, separated, and reutilized from water media by applying an external magnetic field, which results in restricting the production of secondary contaminants and the catalyst loss.

To assess the separation and recombination of photo-induced charge carriers, an Electrochemical Impedance Spectroscopy (EIS) technique was carried out. The EIS test was conducted at the open circuit potential under the UV system. Figure 1A illustrates the Nyquist plots of $FeNi_3/SiO_2/CuS$, $FeNi_3/SiO_2$, and $FeNi_3$ nanocatalysts. The suggested equivalent circuit is included in the inset of Figure 1A, where $CPE_{dl}$, $R_{ct}$, and $R_s$ represent double-layer capacitance, charge transfer resistance, and solvent resistance, respectively. $R_s$ is defined as the first x-intercept of the Nyquist curves. In addition, the semicircle radius denotes the $R_{ct}$ of the as-prepared nanocomposites, which are oppositely dependent on the $e^-/h^+$ recombination rate of the catalysts. According to the obtained plots, one can conclude that the radius size of the nanocomposites diminished in the order of $FeNi_3 > FeNi_3/SiO_2 > FeNi_3/SiO_2/CuS$, illustrating that coating of $SiO_2$ (middle shell) and CuS (outer shell) facilitated the charge transfer kinetic, thus increasing the $e^-/h^+$ separation rate of the FSC composite.

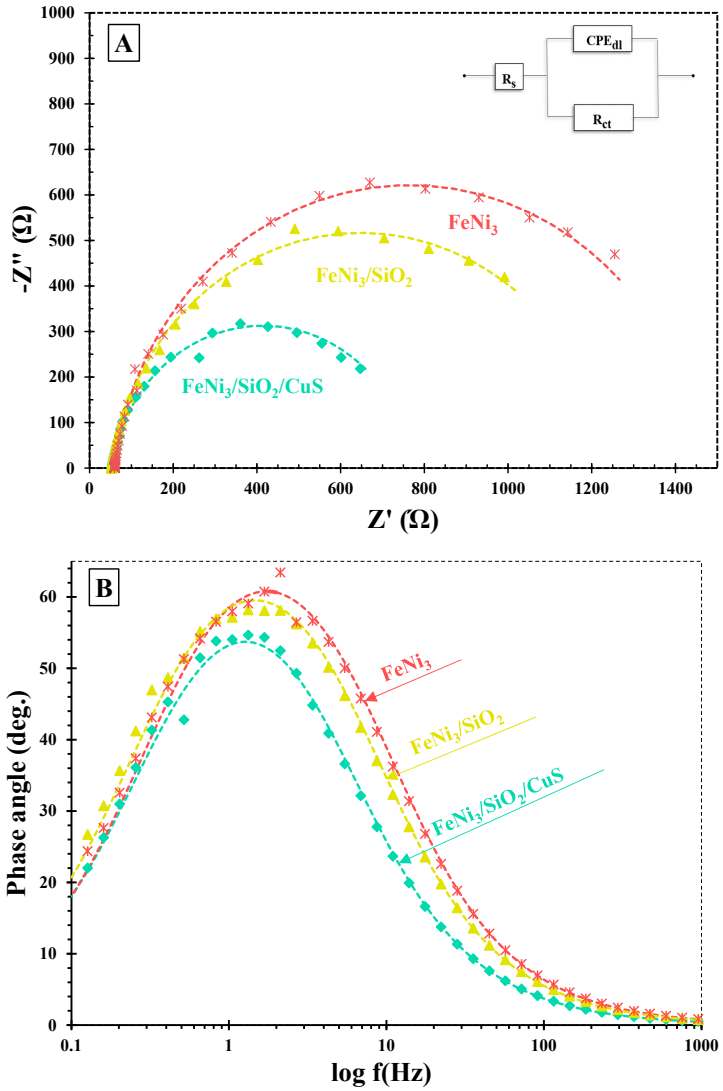



**Figure 1.** (**A**) Nyquist and (**B**) Bode plots of the $FeNi_3/SiO_2/CuS$, $FeNi_3/SiO_2$, and $FeNi_3$ nanocatalysts.

Figure 1B shows the bode plots of the as-synthesized catalysts. Based on the following equation, the carrier lifetime ($\tau_e$) of the mentioned nanocomposites could be determined:

$$\tau_e = 1/\omega_{max} = 1/(2\pi f_{max}) \quad (7)$$

The obtained $\tau_e$ values of the $FeNi_3$, $FeNi_3/SiO_2$, and FSC catalysts were 126.5, 100.4, and 89.5 ms, respectively (see Table 1). These findings showed that the carrier lifetime of the FSC material was higher than the $FeNi_3$ and $FeNi_3/SiO_2$, indicating the introduction of $SiO_2$ and CuS could magnificently improve the electron lifetime. Consequently, one can conclude that the incorporation of $SiO_2$ and CuS into the $FeNi_3$ magnetic core improves the photocatalytic performance of the nanocomposites fabricated in this study, resulting in the higher degradation of TC molecules.

**Table 1.** EIS data of the $FeNi_3/SiO_2/CuS$, $FeNi_3/SiO_2$, and $FeNi_3$ nanocatalysts.

| Catalyst | $f_{max}$ (Hz) | $\tau_e$ (ms) |
|---|---|---|
| $FeNi_3$ | 1.778 | 89.5 |
| $FeNi_3/SiO_2$ | 1.584 | 100.4 |
| $FeNi_3/SiO_2/CuS$ | 1.258 | 126.5 |

### *3.2. Evaluation of the Main Parameters in the Degradation of TC through the $FeNi_3/SiO_2/CuS/UV/H_2O_2$ System*

#### 3.2.1. Impact of Solution pH

In AOPs, the solution pH value is a key factor in the acid–base behavior of contaminants and the surface chemistry of the solid catalyst [44]. Herein, the impact of pH was examined in the range of 3–9, and the findings are displayed in Figure 2. As can be observed, the lowest degradation efficiency of TC was attained at pH = 3 and pH = 9, whereas the highest photocatalytic degradation rate of TC was achieved at a pH of 5 over the $FeNi_3/SiO_2/CuS/UV/H_2O_2$ system. Thus, the optimal pH level of the FSC nanocomposite was in an acid environment.

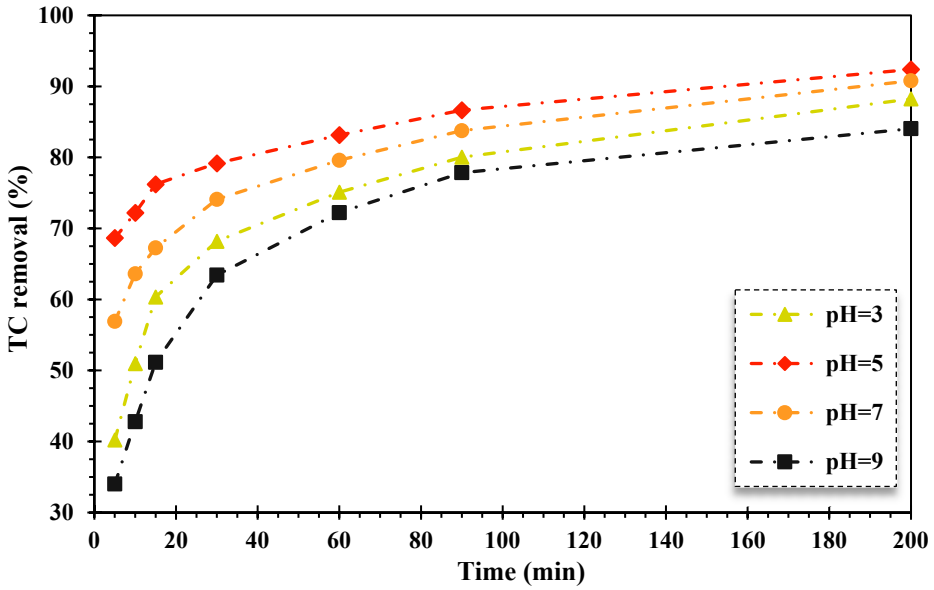



**Figure 2.** The impact of alteration of pH values on the TC elimination efficiency utilizing the $FeNi_3/SiO_2/CuS/UV/H_2O_2$ process (TC content: 20 mg/L, composite quantity: 0.02 g/L, 150 mg/L of $H_2O_2$ concentration).

The acquired results are consistent with similar published reports. Safari et al., (2015) evaluated the decomposition rate of TC using the $TiO_2/UV/H_2O_2$ process from aqueous media [45]. In a similar study, Naddeo et al., (2009) investigated the decomposition

efficiency of diclofenac, carbamazepine, and amoxicillin antibiotics in an aqueous solution under UV radiation. The findings exhibited that the degradation efficiency of the mentioned antibiotics increased with decreasing pH values [46]. Elmolla and Chaudhuri also noted in 2009 that hydrogen peroxide is more stable at low pH values, and oxonium ($H_3O_2^+$) ions improve the stability of $H_2O_2$. As reported, the oxidizing rate of hydroxyl radicals is related to the pH value, which was diminished at alkaline pH values. In 2004, Chu and Wong studied the elimination proportion of the herbicide dicamba using photocatalytic decomposition of $TiO_2$-integrated $H_2O_2$. They stated that its removal efficiency was fallen in alkaline mediums due to the decomposition of $H_2O_2$ into $H_2O$ molecules [47]. Salari et al., (2005) also noted the decomposition rate of intermediates, and subsequently, the target pollutant was decreased in alkaline media utilizing photocatalytic procedures coupled with $H_2O_2$. Therefore, the removal of pollutants is better at acidic pH value in these processes [48]. In addition, in a study conducted by Kumar et al., (2022), the in situ generation of $H_2O_2$ coupled with the Ag/s-($Co_3O_4$/$NiFe_2O_4$) magnetic nanocomposite for photodecomposition of TC was examined under visible light illumination. It was found that the highest production of $H_2O_2$ and maximum elimination efficiency of TC occurred at a pH of 3 during this process [49].

The literature confirmed that the photocatalytic process coupled with $H_2O_2$ causes additional reactions of the composite surface, such as the formation of hydroxide species, leading to a more active site of the nanocomposite for decontaminating pollutants.

#### 3.2.2. Impact of Magnetic Nanocomposite Quantity

To evaluate the impact exerted by the fabricated nanocomposite quantity on the photodecomposition efficiency of TC, a great variety of the FSC dosage was employed in the photocatalytic degradation system when the initial TC content is 20 mg/L, $H_2O_2$ content is 150 mg/L, and pH value is 5.

As displayed in Figure 3, increasing the content of the nanocomposite resulted in the decrease in the TC photo-decontamination rate over the $FeNi_3/SiO_2/CuS/UV/H_2O_2$ system. As the quantity of the synthesized nanocomposite elevated from 0.005 to 0.1 g/L, the decontamination proportion of TC declined from 94.44% to 79.19% during 200 min of degradation time, respectively. This observation can be derived from the declining rate of light penetration through water solutions because of the high concentration of catalyst loading, which induces light scattering and insufficient light absorption on the whole surface particles accessible [50,51].

#### 3.2.3. Impact of TC Content

The influence of initial TC dosage on the decontamination of TC through the heterogeneous Fenton-like photocatalytic system was scrutinized. The initial concentration of TC varied from 20 mg/L to 35 mg/L. The findings are displayed in Figure 4.

As shown in Figure 4, the TC decontamination efficiency diminished by enhancing the TC initial concentration over the $FeNi_3/SiO_2/CuS/UV/H_2O_2$ destruction system. The decrease in the removal rate of TC is attributed to augmenting direct contacts between pollutants and catalysts, which results in inhibitive impacts on photocatalytic reactions and produced oxidizing agents in reaction media. Furthermore, the reduction of illuminating surface catalyst is another factor in declining the photocatalytic oxidation rate of TC with elevating the concentration of TC as a wide number of photons are adsorbed by TC molecules, preventing light influx to the active sites of the catalyst surface [52].

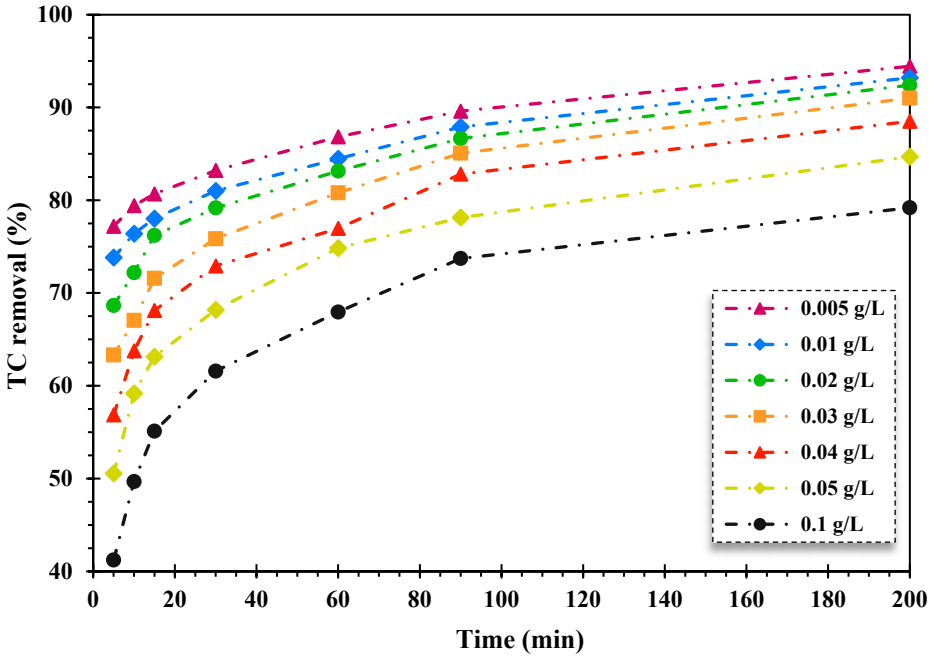



**Figure 3.** The effect of the magnetic nanocatalyst dosage on the percentage of TC removal over the $FeNi_3/SiO_2/CuS/UV/H_2O_2$ process (TC content: 20 mg/L, pH = 5, and $H_2O_2$ content: 150 mg/L).

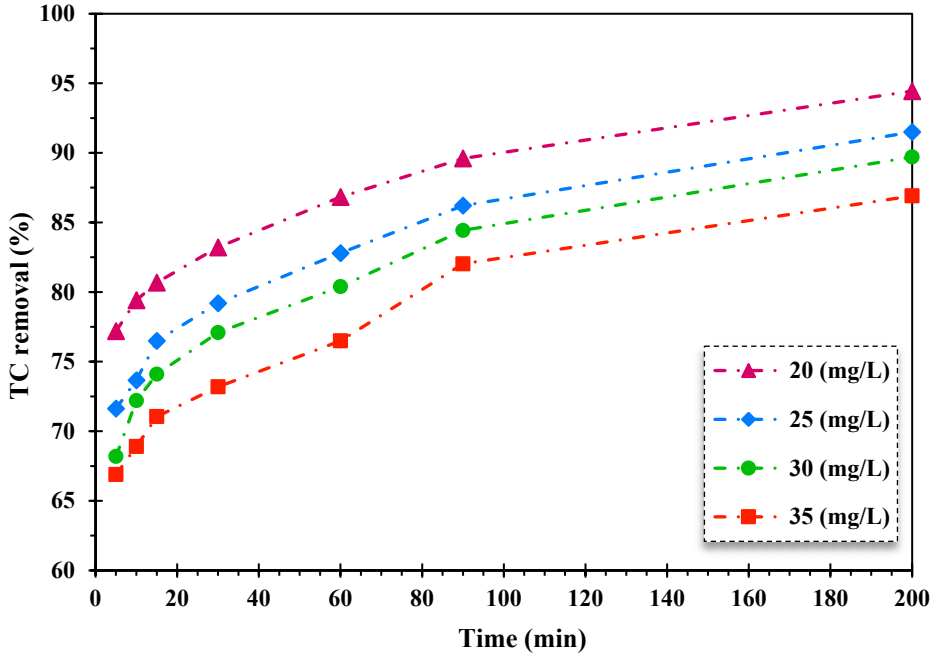



**Figure 4.** The effect of alteration of the initial dosage of TC on its removal efficiency by the $FeNi_3/SiO_2/CuS/UV/H_2O_2$ procedure (5 of pH, 0.005 g/L of catalyst quantity, 150 mg/L of $H_2O_2$ concentration).

### 3.2.4. Impact of $H_2O_2$ Content

To further evaluate the oxidation rate of TC, the effect of $H_2O_2$ dosage (in the range of 50–200 mg/L) and operating time (in 5–200 min) was evaluated over the $FeNi_3/SiO_2/CuS/UV/H_2O_2$ system for the decontamination of TC. For this purpose, the operational parameters (pH, amount of nanocatalyst, and initial concentration of TC) were kept constant at their optimal levels.

Applying the concentration of $H_2O_2$ is a crucial factor in degrading organic matter by Fenton-like processes. This is a dominant source of producing $HO^{\bullet}$ radicals for destructing organic pollutants. As can be seen from Figure 5, the decontamination percentage of contaminants improved by raising the $H_2O_2$ dosage during the Fenton-like process. Furthermore, in most experimental runs, the photocatalytic oxidation rate of TC was enhanced through the addition of $H_2O_2$ concentration. To achieve the highest efficiency of the applied $H_2O_2$ concentration in oxidation systems, it is necessary to determine the optimal content of $H_2O_2$. This oxidant has two roles in the mechanism of the photocatalytic oxidation system, which are formed $HO^{\bullet}$ radicals [53].

$$H_2O_2 + e^- \rightarrow OH^- + HO^{\bullet} \quad (8)$$

$$H_2O_2 + O_2^{\bullet -} \rightarrow HO^{\bullet} + OH^- + O_2 \quad (9)$$

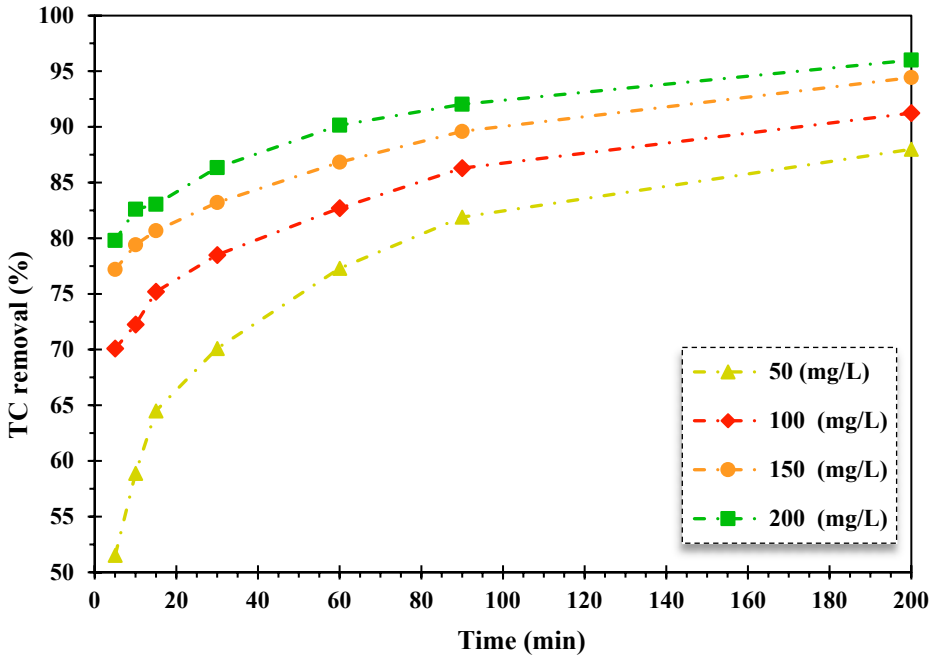



**Figure 5.** The impact of the alteration of $H_2O_2$ quantity on the TC removal efficiency over the $FeNi_3/SiO_2/CuS/UV/H_2O_2$ process (pH = 5, TC content: 20 mg/L, catalyst quantity: 0.005 g/L).

Moreover, hydroxyl radicals are produced with great concentrations of $H_2O_2$ in Fenton-like heterogeneous photocatalytic processes because of the scavenging of $HO^{\bullet}$ radical at its low concentrations. Kakavandi et al., (2016) studied the removal rate of TC utilizing the heterogeneous catalytic photo-Fenton procedure of $Fe_3O_4$@C/UV, which reported that the TC elimination rate enhanced from 43.9%. to 98.4% when the $H_2O_2$ dosage elevated from 1 to 5 mmol [54].

### *3.3. Kinetic Study*

The TC degradation kinetics were investigated by the pseudo-first-order model, which is generally applied to comprehend the decontamination mechanism of contaminants in the treatment system of AOPs [55,56]. This kinetic model was utilized to reveal the speed of the TC decontamination process. The calculated results are displayed in Table 2 and Figure 6. The reaction rate constant ($k_{obs}$) shows a considerable fall with increasing concentration of TC. Nagamine et al. (2020) evaluated the photocatalytic activity of the CdS hydrophilic nanoparticles for the elimination of TC, adopting multiple kinetic models. The results demonstrated that the photo-decomposition of TC was well-described with the

pseudo-first-order reaction kinetic model, which is in line with the obtained findings in the present study [57,58].

**Table 2.** The computed pseudo-first-order kinetic factors for TC decomposition over the $FeNi_3/SiO_2/CuS/UV/H_2O_2$ system.

| Content (mg/L) | Kinetic Equation | $k_0$ (1/min) | $R^2$ | $T_{50\%}$ (min) |
|---|---|---|---|---|
| 20 | y = 0.0071 x + 1.5393 | $7.1 \times 10^{-3}$ | 0.981 | 97.6 |
| 25 | y = 0.006 x + 1.3379 | $6.0 \times 10^{-3}$ | 0.964 | 115.5 |
| 30 | y = 0.0054 x + 1.2502 | $5.4 \times 10^{-3}$ | 0.960 | 128.3 |
| 35 | y = 0.0047 x + 1.1571 | $4.7 \times 10^{-3}$ | 0.954 | 147.4 |
| $T_{50\%} = 0.693/K_0$ | | | | |

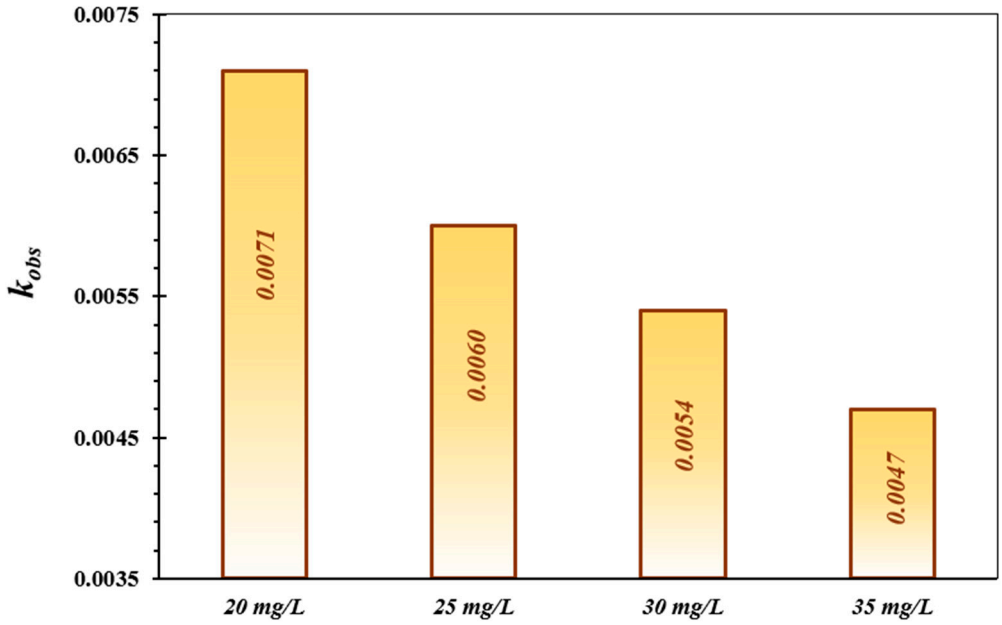



**Figure 6.** Comparison of the photo-decontamination reaction rate constant of TC over the $FeNi_3/SiO_2/CuS/UV/H_2O_2$ process.

### *3.4. Stability and Reusability Study*

To investigate the stability of the FSC composite, TC photo-decontamination experiments were conducted in six consecutive reaction runs under optimized operating circumstances. Based on Figure 7, it is observed that the efficiency of the FSC composite marginally declined by only 4.13% after six continuous cycles. This small decrease in the TC efficiency can be owed to the reduction in the nanocomposite mass during the recycling experiments. According to these outcomes, the FSC composite has great reusability and stability in the photo-decontamination of TC from aqueous environments.

### *3.5. Environmental Risk Assessment*

Consumers are in danger of severe health problems when antibiotics exist in water resources. Based on it, the health risk assessment of the water sample contaminated with TC was conducted through the computation of the HQ index. The HQ level is defined as the ratio of the average daily intake of substance use to a tolerable daily dose by USEPA.

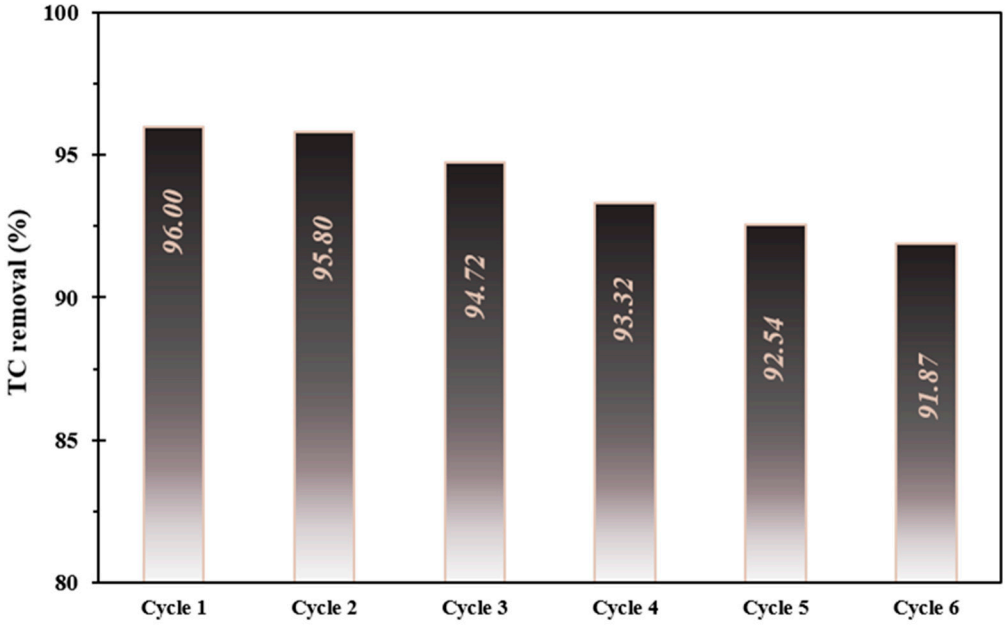



**Figure 7.** The decomposition stability investigation of the as-prepared catalyst at optimized operational conditions.

The HQ level less than or equal to one indicates not many chronic-toxic side-effects on the health consumers. However, matters with HQ values greater than one are shown the harmful risks to the health conditions of consumers. The values of the health risk assessment of TC removal from the investigated water sources are presented in Table 3. Regarding the outcomes, the HQ level was under one after applying the photocatalytic system of UV/$FeNi_3$/$SiO_2$/CuS, which declined considerably with the rise of removal efficiency. The results indicated no TC health risks in the surface water for consumers.

**Table 3.** Health risk levels of TC elimination through multiple photocatalytic procedures from the surface water source at optimized operational factors.

| Oxidation Process | TC Elimination (%) | Tetracycline | | | |
|---|---|---|---|---|---|
| | | CDI (μg/kg d) | | HQ | |
| | | Average | STD | Average | STD |
| **$FeNi_3$** | 49.71 | $1.13 \times 10^{-1}$ | $1.46 \times 10^{-1}$ | $3.78 \times 10^{-1}$ | $4.85 \times 10^{-1}$ |
| **$FeNi_3/SiO_2$** | 70.46 | $5.96 \times 10^{-2}$ | $7.73 \times 10^{-2}$ | $1.99 \times 10^{-1}$ | $2.85 \times 10^{-1}$ |
| **$FeNi_3/SiO_2$/CuS/UV/$H_2O$** | 96 | $8.83 \times 10^{-3}$ | $1.19 \times 10^{-2}$ | $2.94 \times 10^{-2}$ | $3.95 \times 10^{-2}$ |

Although environmental studies have been limited to investigating human health risks of water sources after advanced water treatment methods, Amarzadeh et al. researched the health risk assessments in the drinking water sample contaminated with ciprofloxacin and penicillin after the integration treatment process based on AOPs [59]. The main results of their study exhibited a suitable level of HQ and CDI, which is consistent with the findings of the present work.

### *3.6. Impact of Trapping Agents*

As presented in Figure 8, the decontamination efficiency of TC was 96% via the $FeNi_3$/$SiO_2$/CuS/UV/$H_2O_2$ system in the absence of quenchers, while the introduction of IPA, EDTA, chloroform, and $K_2S_2O_8$ was deteriorated the elimination proportion to 48.53%, 66.67%, 80.53%, and 95.86%, respectively. The findings demonstrated that $HO^{\bullet}$ radicals are the predominant oxidizing species accounting for the photodegradation of TC.

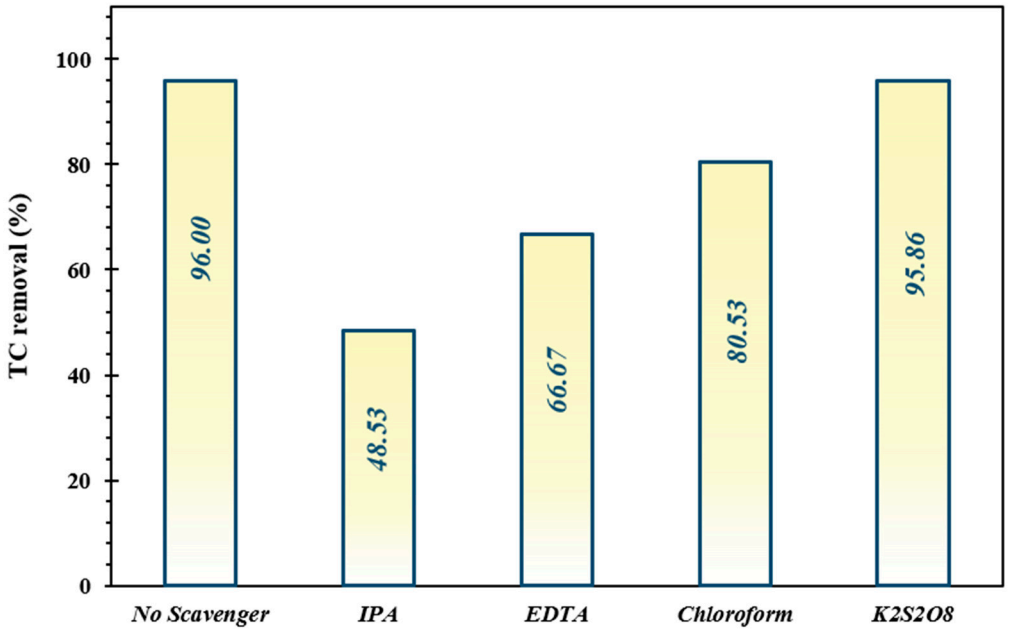



**Figure 8.** Impact of trapping agents (IPA, EDTA, chloroform, and $K_2S_2O_8$) on decomposition performance of TC under optimized operating conditions.

### *3.7. Comparative Experiments on TC Degradation*

In AOPs, various types of mechanisms may be involved simultaneously in the degradation of pollutants; thus, determining the ratio of each mechanism is a crucial issue in evaluating the synergistic effect [60]. In this regard, the efficiency of different systems in the decomposition of TC antibiotics was studied under the same operational circumstances within 200 min of reaction time, and the obtained outcomes are shown in Figure 9. According to the results, $FeNi_3/SiO_2/CuS/UV/H_2O_2$ system had the greatest decontamination efficiency (96%), which indicated that the adsorption by FCS and oxidative decomposition under $H_2O_2$ and UV illumination had a positive synergy on the TC degradation system. In contrast, the low efficiencies of 14% and 30% were obtained for single UV and $H_2O_2$, demonstrating the insignificant oxidation potential of these systems in the decomposition of TC antibiotics. Moreover, FSC/UV and $UV/H_2O_2$ processes with TC decontamination efficiencies of 62 and 49%, respectively, had greater performance in the removal of contaminants compared to single processes. One can observe that by coupling UV and $H_2O_2$, TC degradation efficiency was greatly enhanced (49%), which demonstrated the presence of positive synergism between UV and $H_2O_2$. Indeed, $H_2O_2$ molecules can be decomposed to $HO^{\bullet}$ in the presence of UV light. In the case of UV/FSC, the decontamination efficiency of TC was magnificently increased (62%) compared to FSC alone, revealing that the mentioned nanocomposite has a photocatalytic activity in the presence of UV, owing to the excitation of FSC electrons. On the other hand, a greater degradation rate of the $UV/H_2O_2$ process than $FSC/H_2O_2$ indicated that the capability of UV illumination for activation of $H_2O_2$ molecules is more than FSC composite. Based on the achieved results, the catalytic potential (CP) of the $FeNi_3/SiO_2/CuS/UV/H_2O_2$ system was studied. As can be seen from Equation (10), by comparing the degradation performance of the main system with those obtained by individual FSC, $H_2O_2$, and UV systems, the catalytic potential could be determined:

$$CP\ (\%) = R_{(FSC/UV/H_2O_2)} - (R_{(FSC)} + R_{(UV)} + R_{(H_2O_2)}) \quad (10)$$

where R is the TC degradation efficiency of each system.

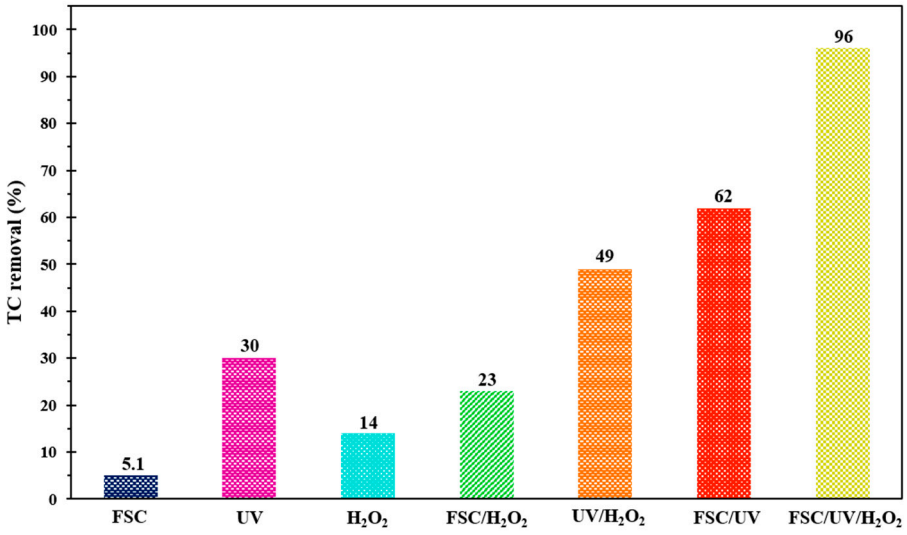



**Figure 9.** TC decomposition rate over multiple processes under similar operating circumstances.

The CP of 47% was obtained for FSC through FSC/UV/$H_2O_2$ process for decomposing TC illustrating that the coupling of FSC with $H_2O_2$ and UV light, owing to the magnificent synergistic effect, can be considered an effective approach for the removal of antibiotics. To validate the presence of positive synergism in the FSC/UV/$H_2O_2$ process, an enhancement factor (R) was defined based on the TC decontamination performance of binary (FSC/$H_2O_2$ and UV/$H_2O_2$) and ternary (FSC/UV/$H_2O_2$) systems (Equation (11)):

$$\text{Enhancement factor (R)} = \frac{\text{TC decompostion via FSC/UV/H}_2\text{O}_2\text{ system}}{\text{TC decompostion via [(FSC/H}_2\text{O}_2\text{) + (UV/H}_2\text{O}_2\text{)] systems}} \quad (11)$$

According to the abovementioned relation, the value of R was found to be >1.0 (R = 1.33) for FSC/UV/$H_2O_2$ system, which confirms the magnificent synergistic effect between applied systems. Hence, the FSC/UV/$H_2O_2$ system was selected as an ideal process in TC degradation among all individual processes.

### *3.8. Mineralization*

Mineralization is regarded as the decomposition of stubborn pollutants into $CO_2$, $H_2O$, and inorganic matter [61]. Complete mineralization of pollutants can quite impossible using simple water systems. Herein, to investigate the performance of the FSC/UV/$H_2O_2$ system for TC detoxification, the mineralization degree was investigated via TOC under optimized operational circumstances. As displayed in Figure 10, with elevating operating time up to 90 min, The TOC elimination efficiency was enhanced remarkably, which reached 70%. According to the outcomes, the insufficient decay rate of TC compared to decomposition one was ascribed to the formation of intermediate by-products throughout the decontamination of TC that contributes to the aliquot of TOC.

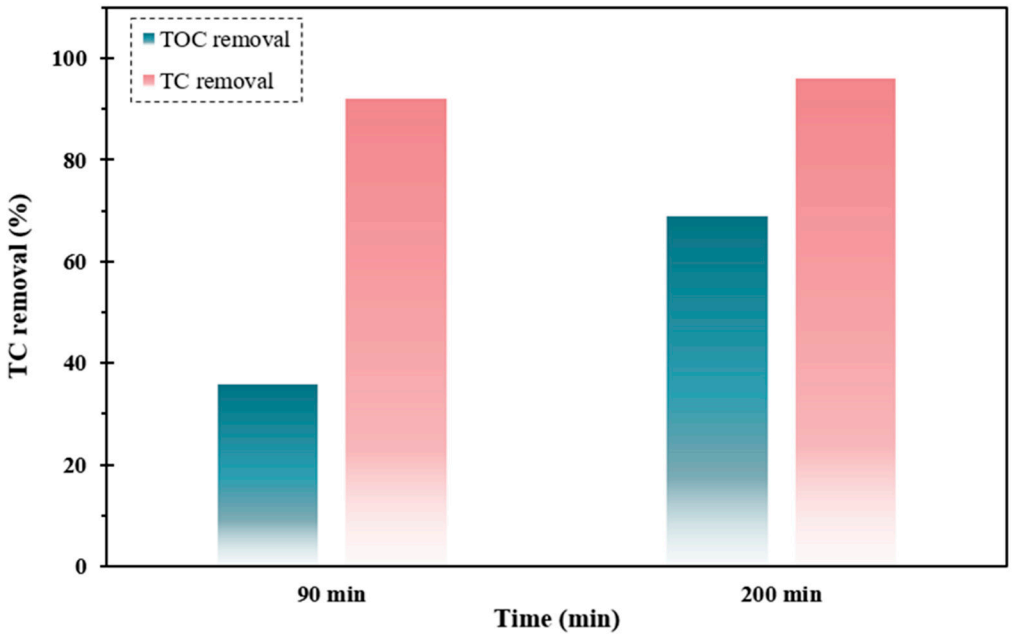
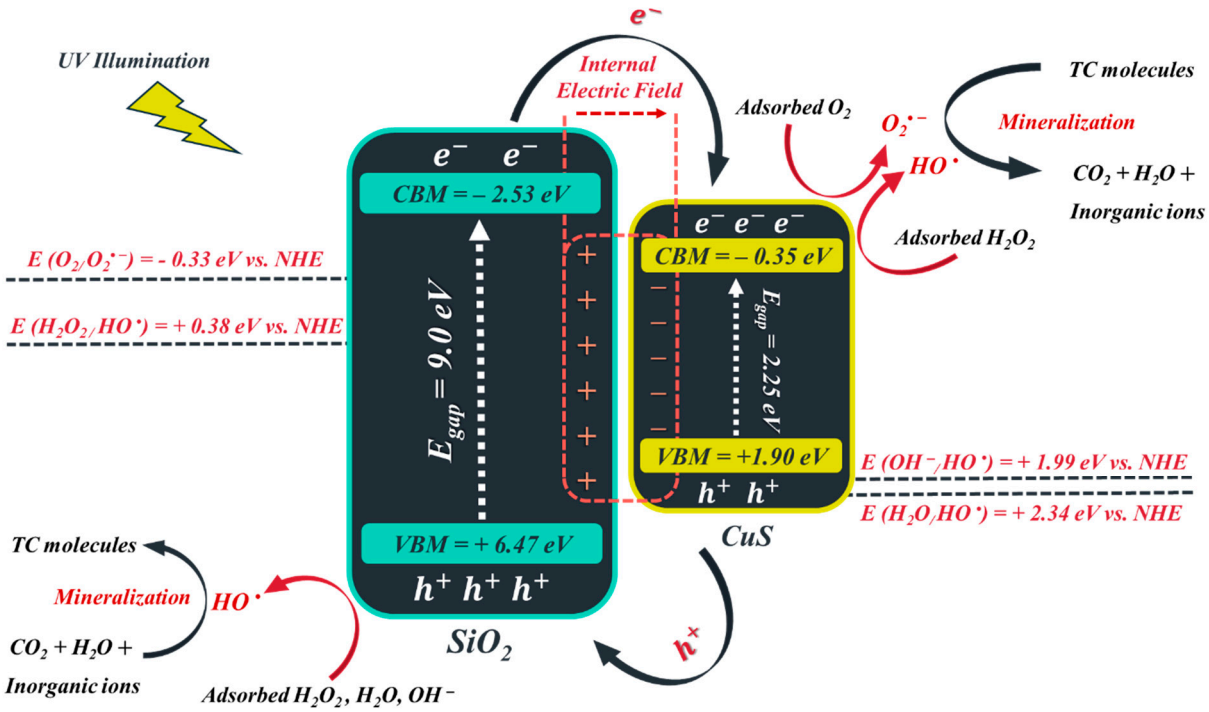



**Figure 10.** TC and TOC elimination profiles by FSC/UV/$H_2O_2$ system under optimized operating circumstances.

### *3.9. Mechanism of TC Decomposition over $FeNi_3/SiO_2/CuS/UV/H_2O_2$ System*

In this study, the probable mechanism for TC photocatalytic decontamination over FSC nanocomposite in the presence of UV light was scrutinized, which is illustrated in Scheme 1:




**Scheme 1.** The probable photocatalytic mechanism for TC decontamination using the $FeNi_3/SiO_2/CuS/UV/H_2O_2$ system.

As indicated previously, $FeNi_3$ was used as a magnetic core so that the synthesized FSC nanocomposite could be easily separated from the reaction mixture by using a strong magnetic field. On the other hand, $SiO_2$ and CuS nanomaterials were utilized as photocatalysts to decompose the TC molecules. However, note that the main role of $SiO_2$ (middle shell)

was to reduce the attraction among $FeNi_3$ particles and also to protect them from oxidation. Semiconductors possess two types of charge carriers: (I) $e^-$ in the conduction band minima (CBM) and (II) $h^+$ in the valence band maxima (VBM). The energy range between CBM and VBM is called "the band gap". When CuS and $SiO_2$ nanoparticles are exposed to UV irradiation, whose energy is higher than the bandgap of the CuS (2.25 eV) and $SiO_2$ (9 eV), the photons transfer $e^-$ from the VBM of these semiconductors to the CBM, which results in the generation of $h^+$ in the VBM (Equation (12)).

$$\text{UV Irradiation} + \text{FSC nanocomopsite} \rightarrow \text{FSC}\left(e^- + h^+\right) \quad (12)$$

To assess the enhanced photocatalytic activity of the FSC catalyst, it is vital to determine the location of CBM and VBM of CuS and $SiO_2$ semiconductors. The energy levels of the as-mentioned semiconductors can be determined using the following relations (Equations (13) and (14)):

$$\text{VBM} = \frac{E_{gap}}{2} + x - E_e \quad (13)$$

$$\text{CBM} = \text{VBM} - E_{gap} \quad (14)$$

where $\chi$ = the absolute electronegativity of the photocatalysts;

$E_e$ = the energy of free electrons (~4.5 eV);
$E_{gap}$ = the band gap of the synthesized catalysts;
VBM = Valence band potential of the synthesized catalysts;
CBM = Conduction band potential of the synthesized catalysts.

According to our previously published works, the bandgap of CuS and $SiO_2$ were found to be 2.25 and 9 eV [62,63]. In addition, the X values of CuS and $SiO_2$ semiconductors were 5.28 and 6.47, respectively. By adding these data to the aforementioned relations, the VBM and CBM of CuS and $SiO_2$ nanomaterials can be determined, which are illustrated in Table 4. Based on Scheme 1, as the FSC nanocomposite is illuminated with the photons of the UV light, the electrons of CuS and $SiO_2$ are excited, and thereby, the holes are generated in the VBM. One can observe that the CBM and VBM of $SiO_2$ catalyst (−2.53 and 6.47 eV, respectively) are, respectively, smaller and greater than the CBM and VBM of CuS semiconductor (−0.35 and 1.90 eV, respectively). CuS-$SiO_2$ is a p-n type heterojunction, which is capable of accelerating the migration of charge carriers across the heterojunction to enhance the TC decomposition potential by generating an internal electric field directed from $SiO_2$ to CuS. In this regard, under UV illumination, the photo-induced electrons of the $SiO_2$ semiconductor will possibly migrate to the CBM of CuS. Since the CBM of CuS (−0.35 eV) is more negative than the redox potential of $O_2/O_2^{\bullet -}$ (−0.33 eV vs. NHE), it can be expected that the accumulated electrons in CBM of CuS to participate in redox reaction for the generation of intermediates such as $O_2^{\bullet -}$, $HO_2^{\bullet}$, $HO^{\bullet}$, and $H_2O_2$ (Equations (15)–(21)) [64,65].

$$O_2 + e^- \rightarrow O_2^{\bullet -} \quad (15)$$

$$O_2^{\bullet -} + H^+ \rightarrow HO_2^{\bullet} \quad (16)$$

$$O_2^{\bullet -} + 2H^+ + e^- \rightarrow H_2O_2 \quad (17)$$

$$O_2^{\bullet -} + H_2O \rightarrow HO_2^{\bullet} + OH^- \quad (18)$$

$$O_2^{\bullet -} + H_2O_2 \rightarrow OH^- + HO^{\bullet} + O_2 \quad (19)$$

$$2HO_2^{\bullet} \rightarrow H_2O_2 + O_2 \quad (20)$$

$$HO_2^{\bullet} + H^+ + e^- \rightarrow H_2O_2 \quad (21)$$

**Table 4.** VBM, CBM, and $E_{gap}$ of CuS and $SiO_2$ semiconductors.

| Catalyst | $E_{gap}$ (eV vs. NHE) | VBM (eV vs. NHE) | CBM (eV vs. NHE) |
|---|---|---|---|
| CuS | 2.25 | 1.90 | −0.35 |
| $SiO_2$ | 9 | 6.47 | −2.53 |

However, the photo-induced holes on the VBM of $SiO_2$ were incapable of transferring to the VBM of CuS owing to the repulsive force of the generated electric field, which resulted in the diminution of the $e^-/h^+$ recombination rate. This outcome is in complete agreement with the results obtained by the EIS test. Note that the induced holes in VBM of $SiO_2$ can decompose TC molecules and react with $OH^-$ and $H_2O$ to form $OH^\bullet$ (Equations (22) and (23)), as a consequence of more positive VBM of $SiO_2$ (6.47 eV) than the redox potential of $OH^\bullet/OH^\bullet$ (1.99 eV vs. NHE) and $H_2O/OH^\bullet$ (2.34 eV vs. NHE).

$$\left(h^+\right) + OH^- \rightarrow HO^\bullet \quad (22)$$

$$\left(h^+\right) + H_2O \rightarrow HO^\bullet + H^+ \quad (23)$$

Moreover, the added and the generated $H_2O_2$ could also form $HO^\bullet$ by reacting with excited $h^+$ and $e^-$ on the catalyst surface or by adsorption of light illumination (Equations (24)–(26)) [65].

$$H_2O_2 + e^- \rightarrow OH^- + HO^\bullet \quad (24)$$

$$H_2O_2 + \left(h^+\right) \rightarrow 2HO^\bullet \quad (25)$$

$$H_2O_2 \overset{h\vartheta}{\rightarrow} 2HO^\bullet \quad (26)$$

Eventually, these generated reactive species come into contact with the adsorbed TC molecules and form intermediates, which further decompose to $CO_2$, $H_2O$, $NH_4{}^+$, $NO_3{}^-$, $NO_2{}^-$, and $SO_4{}^{2-}$ (Equation (27)).

$$\text{Tetracycline} + \text{Oxidative radicals}\left(O_2^{\bullet-},\ HO^\bullet \text{ and } HO_2^\bullet\right) \rightarrow \text{Intermediates} \rightarrow CO_2 + H_2O + NH_4^+ + NO_3^- + NO_2^- + SO_4^{2-} \quad (27)$$

To summarize, for TC molecules to decompose in the presence of FSC composite and UV light, six main steps must be done: (I) absorption of light by FSC catalyst, (II) generation of $e^-/h^+$ pairs, (III) transferring and recombination of the photo-induced $e^-/h^+$ pairs, (IV) adsorption of $H_2O$, $OH^-$, $O_2$ and $H_2O_2$ molecules on the surface of the catalyst, (V) participation of photo-induced electrons and holes in the redox reaction to form reactive radicals, and (VI) desorption of generated radicals.

$$CP\ (\%) = R_{(FSC/UV/H_2O_2)} - \left(R_{(FSC)} + R_{(UV)} + R_{(H_2O_2)}\right)$$

## 4. Conclusions

This study purposed to scrutinize the photocatalytic function of FSC composite in eliminating TC from aqueous solutions exposed to UV and $H_2O_2$. The findings showed that this system had an excellent degradation rate of TC (96%) under optimal operating circumstances (pH = 5, the catalyst dose of 0.005 g/L, 200 min of operating time, and 20 mg/L of TC content, and $H_2O_2$ quantity = 200 mg/L. The results also exhibited that the composite dosage and the TC content had negative effects on the procedure function in the way that the decomposition rate of TC declined considerably, as both contents enhanced the decomposition rate of TC. In addition, the outcomes revealed that the elimination proportion of TC by the alone application of hydrogen peroxide and UV accounted for 14% and 30%, respectively. Based on the kinetic calculations of the reaction rate, it was determined that the integration of the photocatalytic system of UV/$FeNi_3$/$SiO_2$/CuS with

hydrogen peroxide is well-fitted to the pseudo-first-order model. Furthermore, to demonstrate the stability and reusability of the as-prepared nanocatalyst, cycling experiments were conducted for six cycles, exhibiting a slight decrease in the elimination rate of TC. Therefore, according to the aforementioned outcomes, the photocatalytic integration process with $H_2O_2$ as $FeNi_3/SiO_2/CuS/UV/H_2O_2$ has a great photodegradation ability for eradicating a wide variety of compounds-contained pharmaceutical effluents. In the end, it is suggested to verify the potential capability of this process on a real scale, the remediation system of $FeNi_3/SiO_2/CuS/UV/H_2O_2$ should be examined for purifying real wastewater.

**Author Contributions:** Methodology, M.A. (Mohammadamin Amarzadeh), M.A. (Moslem Azqandi) and N.N.; Formal analysis, M.A. (Mohammadamin Amarzadeh) and M.A. (Moslem Azqandi); Investigation, N.N.; Writing—original draft, M.A. (Mohammadamin Amarzadeh), M.A. (Moslem Azqandi), K.N., B.R. and N.N.; Writing—review & editing, M.A. (Mohammadamin Amarzadeh), B.R.; Supervision, N.N. and N.A.K.; Project administration, N.N. and N.A.K.; Funding acquisition, N.A.K. All authors have read and agreed to the published version of the manuscript.

**Funding:** This research received no external funding.

**Institutional Review Board Statement:** Not applicable.

**Data Availability Statement:** Not applicable.

**Acknowledgments:** The authors express their sincere thanks to Birjand University of Medical Sciences for the support extended for the production of this paper. The Ethics Committee of Birjand University of Medical Sciences (Iran) approved the study with the ethical code IR.BUMS.REC.1401.296.

**Conflicts of Interest:** The authors declare no conflict of interest.

## References

1. Xiang, W.; Yuan, J.; Wu, Y.; Luo, H.; Xiao, C.; Zhong, N.; Zhao, M.; Zhong, D.; He, Y. Working principle and application of photocatalytic optical fibers for the degradation and conversion of gaseous pollutants. *Chin. Chem. Lett.* **2022**, *33*, 3632–3640. [CrossRef]
2. Li, G.; Huang, S.; Li, K.; Zhu, N.; Zhao, B.; Zhong, Q.; Zhang, Z.; Ge, D.; Wang, D. Near-infrared responsive Z-scheme heterojunction with strong stability and ultra-high quantum efficiency constructed by lanthanide-doped glass. *Appl. Catal. B Environ.* **2022**, *311*, 121363. [CrossRef]
3. Jeong, J.; Song, W.; Cooper, W.J.; Jung, J.; Greaves, J. Degradation of tetracycline antibiotics: Mechanisms and kinetic studies for advanced oxidation/reduction processes. *Chemosphere* **2010**, *78*, 533–540. [CrossRef] [PubMed]
4. Xia, T.; Lin, Y.; Li, W.; Ju, M. Photocatalytic degradation of organic pollutants by MOFs based materials: A review. *Chin. Chem. Lett.* **2021**, *32*, 2975–2984. [CrossRef]
5. Zhang, G.; Zhao, Z.; Yin, X.-A.; Zhu, Y. Impacts of biochars on bacterial community shifts and biodegradation of antibiotics in an agricultural soil during short-term incubation. *Sci. Total. Environ.* **2021**, *771*, 144751. [CrossRef]
6. Liu, C.; Mao, S.; Wang, H.; Wu, Y.; Wang, F.; Xia, M.; Chen, Q. Peroxymonosulfate-assisted for facilitating photocatalytic degradation performance of 2D/2D $WO_3$/BiOBr S-scheme heterojunction. *Chem. Eng. J.* **2021**, *430*, 132806. [CrossRef]
7. Chen, Z.; Lin, B.; Huang, Y.; Liu, Y.; Wu, Y.; Qu, R.; Tang, C. Pyrolysis temperature affects the physiochemical characteristics of lanthanum-modified biochar derived from orange peels: Insights into the mechanisms of tetracycline adsorption by spectroscopic analysis and theoretical calculations. *Sci. Total. Environ.* **2023**, *862*, 160860. [CrossRef] [PubMed]
8. Miyata, M.; Ihara, I.; Yoshid, G.; Toyod, K.; Umetsu, K. Electrochemical oxidation of tetracycline antibiotics using a Ti/$IrO_2$ anode for wastewater treatment of animal husbandry. *Water Sci. Technol.* **2011**, *63*, 456–461. [CrossRef] [PubMed]
9. Kamiya, T.; Hirotsuji, J. New combined system of biological process and intermittent ozonation for advanced wastewater treatment. *Water Sci. Technol.* **1998**, *38 Pt 7*, 145–153. [CrossRef]
10. Qi, C.; Wen, Y.; Zhao, Y.; Dai, Y.; Li, Y.; Xu, C.; Yang, S.; He, H. Enhanced degradation of organic contaminants by Fe(III)/peroxymonosulfate process with l-cysteine. *Chin. Chem. Lett.* **2022**, *33*, 2125–2128. [CrossRef]
11. Peng, J.; Wang, Z.; Wang, S.; Liu, J.; Zhang, Y.; Wang, B.; Gong, Z.; Wang, M.; Dong, H.; Shi, J.; et al. Enhanced removal of methylparaben mediated by cobalt/carbon nanotubes (Co/CNTs) activated peroxymonosulfate in chloride-containing water: Reaction kinetics, mechanisms and pathways. *Chem. Eng. J.* **2021**, *409*, 128176. [CrossRef]
12. Cao, H.; Dai, Y.; Wu, L.; Qi, C.; Hou, L.; Zhang, D.; Li, Y.; Xu, C.; He, H.; Yang, S. Degradation of iohexol in the Co(II)/peracetic acid system under neutral conditions: Influencing factors, degradation pathways and toxicity. *Sep. Purif. Technol.* **2023**, *319*, 124083. [CrossRef]
13. Dai, Y.; Cao, H.; Qi, C.; Zhao, Y.; Wen, Y.; Xu, C.; Zhong, Q.; Sun, D.; Zhou, S.; Yang, B.; et al. L-cysteine boosted Fe(III)-activated peracetic acid system for sulfamethoxazole degradation: Role of L-cysteine and mechanism. *Chem. Eng. J.* **2023**, *451*, 138588. [CrossRef]

14. Che, H.; Che, G.; Jiang, E.; Liu, C.; Dong, H.; Li, C. A novel Z-Scheme CdS/Bi3O4Cl heterostructure for photocatalytic degradation of antibiotics: Mineralization activity, degradation pathways and mechanism insight. *J. Taiwan Inst. Chem. Eng.* **2018**, *91*, 224–234. [CrossRef]
15. Khan, S.B.; Irfan, S.; Lam, S.S.; Sun, X.; Chen, S. 3D printed nanofiltration membrane technology for waste water distillation. *J. Water Process. Eng.* **2022**, *49*, 102958. [CrossRef]
16. Ye, Y.; Yang, P.; Deng, Y.; Yang, Y.; Zhang, K.; Wang, Y.; Shang, W.; Li, Q.; Sun, L.; Pan, F.; et al. Non-woven cotton fabric based intimately coupling of photocatalysis and biodegradation system for efficient removal of Cu(II) complex in water. *Chin. Chem. Lett.* **2022**, *33*, 3127–3132. [CrossRef]
17. Eskandarinezhad, S.; Khosravi, R.K.R.; Amarzadeh, M.; Mondal, P.; Filho, F.J.C.M. Application of different Nanocatalysts in industrial effluent treatment: A review. *J. Compos. Compd.* **2021**, *2*, 43–56. [CrossRef]
18. Xia, G.; Zheng, Y.; Sun, Z.; Xia, S.; Ni, Z.; Yao, J. Fabrication of ZnAl-LDH mixed metal-oxide composites for photocatalytic degradation of 4-chlorophenol. *Environ. Sci. Pollut. Res.* **2022**, *29*, 39441–39450. [CrossRef]
19. Yu, H.; Zhu, J.; Qiao, R.; Zhao, N.; Zhao, M.; Kong, L. Facile Preparation and Controllable Absorption of a Composite Based on $PMo_{12}$/Ag Nanoparticles: Photodegradation Activity and Mechanism. *Chemistryselect* **2022**, *7*, e202103668. [CrossRef]
20. Chen, F.; Zhang, Y.; Huang, H. Layered photocatalytic nanomaterials for environmental applications. *Chin. Chem. Lett.* **2023**, *34*, 107523. [CrossRef]
21. Kamranifar, M.; Allahresani, A.; Naghizadeh, A. Synthesis and characterizations of a novel $CoFe_2O_4$@CuS magnetic nanocomposite and investigation of its efficiency for photocatalytic degradation of penicillin G antibiotic in simulated wastewater. *J. Hazard. Mater.* **2018**, *366*, 545–555. [CrossRef]
22. Shi, W.; Ren, H.; Li, M.; Shu, K.; Xu, Y.; Yan, C.; Tang, Y. Tetracycline removal from aqueous solution by visible-light-driven photocatalytic degradation with low cost red mud wastes. *Chem. Eng. J.* **2010**, *382*, 122876. [CrossRef]
23. Kakavandi, B.; Bahari, N.; Kalantary, R.R.; Fard, E.D. Enhanced sono-photocatalysis of tetracycline antibiotic using $TiO_2$ decorated on magnetic activated carbon (MAC@T) coupled with US and UV: A new hybrid system. *Ultrason. Sonochem.* **2019**, *55*, 75–85. [CrossRef]
24. Martins, A.C.; Cazetta, A.L.; Pezoti, O.; de Souza, J.R.B.; Zhang, T.; Pilau, E.; Asefa, T.; Almeida, V.C. Sol-gel synthesis of new $TiO_2$/activated carbon photocatalyst and its application for degradation of tetracycline. *Ceram. Int.* **2016**, *43*, 4411–4418. [CrossRef]
25. Gao, X.; E Wachs, I. Titania–silica as catalysts: Molecular structural characteristics and physico-chemical properties. *Catal. Today* **1999**, *51*, 233–254. [CrossRef]
26. Belver, C.; Bedia, J.; Rodriguez, J. Titania–clay heterostructures with solar photocatalytic applications. *Appl. Catal. B Environ.* **2015**, *176–177*, 278–287. [CrossRef]
27. Guo, W.; Luo, H.; Jiang, Z.; Fang, D.; Chi, J.; Shangguan, W.; Wang, Z.; Wang, L.; Lee, A.F. Ge-Doped Cobalt Oxide for Electrocatalytic and Photocatalytic Water Splitting. *ACS Catal.* **2022**, *12*, 12000–12013. [CrossRef]
28. Zuo, L.; Yu, S.; Zhang, R.; Li, H.; Wu, Y.; Abiev, R.; Sun, Z.; Sun, Z. Tunning Pd–Cu-based catalytic oxygen carrier for intensifying low-temperature methanol reforming. *J. Clean. Prod.* **2023**, *410*, 137212. [CrossRef]
29. Primo, O.; Rivero, M.J.; Ortiz, I. Photo-Fenton process as an efficient alternative to the treatment of landfill leachates. *J. Hazard. Mater.* **2008**, *153*, 834–842. [CrossRef] [PubMed]
30. Wang, R.; Liu, X.; Wu, R.; Yu, B.; Li, H.; Zhang, X.; Xie, J.; Yang, S.-T. $Fe_3O_4/SiO_2$/C nanocomposite as a high-performance Fenton-like catalyst in a neutral environment. *RSC Adv.* **2016**, *6*, 8594–8600. [CrossRef]
31. Zhang, Q.; Zhang, A.; Li, H.; Zhang, X.; Sun, Z.; Mei, Y.; Xiang, J.; Su, S.; Tan, Z.; Lu, H. $FeNi_3$ foam as cathode catalyst in electrocatalytic peroxydisulfate system for enhanced Hg0 removal from simulated flue gas. *J. Environ. Chem. Eng.* **2023**, *11*, 109384. [CrossRef]
32. Saberi, S.; Zhiani, R.; Mehrzad, J.; Motavalizadehkakhky, A. Synthesis and characterization of a novel TEMPO@$FeNi_3$/DFNS–laccase magnetic nanocomposite for the reduction of nitro compounds. *RSC Adv.* **2020**, *10*, 27297–27304. [CrossRef]
33. Shekari, H.; Sayadi, M.; Rezaei, M.; Allahresani, A. Synthesis of nickel ferrite/titanium oxide magnetic nanocomposite and its use to remove hexavalent chromium from aqueous solutions. *Surfaces Interfaces* **2017**, *8*, 199–205. [CrossRef]
34. Narzary, S.; Alamelu, K.; Raja, V.; Ali, B.J. Visible light active, magnetically retrievable $Fe_3O_4$@$SiO_2$@g-$C_3N_4/TiO_2$ nanocomposite as efficient photocatalyst for removal of dye pollutants. *J. Environ. Chem. Eng.* **2020**, *8*, 104373. [CrossRef]
35. Farooghi, A.; Sayadi, M.H.; Rezaei, M.R.; Allahresani, A. An efficient removal of lead from aqueous solutions using FeNi 3 @SiO 2 magnetic nanocomposite. *Surfaces Interfaces* **2018**, *10*, 58–64. [CrossRef]
36. Alwared, A.I.; Sulaiman, F.A.; Raad, H.; Al-Musawi, T.J.; Mohammed, N.A. Ability of $FeNi_3/SiO_2/TiO_2$ nanocomposite to degrade amoxicillin in wastewater samples in solar light-driven processes. *South Afr. J. Bot.* **2023**, *153*, 195–202. [CrossRef]
37. Kamranifar, M.; Al-Musawi, T.J.; Amarzadeh, M.; Hosseinzadeh, A.; Nasseh, N.; Qutob, M.; Arghavan, F.S. Quick adsorption followed by lengthy photodegradation using $FeNi_3$@$SiO_2$@ZnO: A promising method for complete removal of penicillin G from wastewater. *J. Water Process. Eng.* **2021**, *40*, 101940. [CrossRef]
38. Nasseri, M.A.; Sadeghzadeh, S.M. A highly active $FeNi_3$–$SiO_2$ magnetic nanoparticles catalyst for the preparation of 4H-benzo[b]pyrans and Spirooxindoles under mild conditions. *J. Iran. Chem. Soc.* **2013**, *10*, 1047–1056. [CrossRef]
39. Geng, N.; Chen, W.; Xu, H.; Ding, M.; Lin, T.; Wu, Q.; Zhang, L. Insights into the novel application of Fe-MOFs in ultrasound-assisted heterogeneous Fenton system: Efficiency, kinetics and mechanism. *Ultrason. Sonochem.* **2021**, *72*, 105411. [CrossRef]

40. Eslami, A.; Amini, M.M.; Yazdanbakhsh, A.R.; Mohseni-Bandpei, A.; A Safari, A.; Asadi, A. N,S co-doped $TiO_2$ nanoparticles and nanosheets in simulated solar light for photocatalytic degradation of non-steroidal anti-inflammatory drugs in water: A comparative study. *J. Chem. Technol. Biotechnol.* **2015**, *91*, 2693–2704. [CrossRef]
41. Wan, Z.; Zhang, T.; Liu, Y.; Liu, P.; Zhang, J.; Fang, L.; Sun, D. Enhancement of desulfurization by hydroxyl ammonium ionic liquid supported on active carbon. *Environ. Res.* **2022**, *213*, 113637. [CrossRef] [PubMed]
42. Semerjian, L.; Shanableh, A.; Semreen, M.H.; Samarai, M. Human health risk assessment of pharmaceuticals in treated wastewater reused for non-potable applications in Sharjah, United Arab Emirates. *Environ. Int.* **2018**, *121*, 325–331. [CrossRef] [PubMed]
43. Nasseh, N.; Arghavan, F.S.; Rodriguez-Couto, S.; Panahi, A.H. Synthesis of $FeNi_3/SiO_2/CuS$ magnetic nano-composite as a novel adsorbent for Congo Red dye removal. *Int. J. Environ. Anal. Chem.* **2022**, *102*, 2342–2362. [CrossRef]
44. Li, T.; Pang, H.; Wu, Q.; Huang, M.; Xu, J.; Zheng, L.; Wang, B.; Qiao, Y. Rigid Schiff Base Complex Supermolecular Aggregates as a High-Performance pH Probe: Study on the Enhancement of the Aggregation-Caused Quenching (ACQ) Effect via the Substitution of Halogen Atoms. *Int. J. Mol. Sci.* **2022**, *23*, 6259. [CrossRef] [PubMed]
45. Safari, G.; Hoseini, M.; Seyedsalehi, M.; Kamani, H.; Jaafari, J.; Mahvi, A.H. Photocatalytic degradation of tetracycline using nanosized titanium dioxide in aqueous solution. *Int. J. Environ. Sci. Technol.* **2015**, *12*, 603–616. [CrossRef]
46. Naddeo, V.; Meriç, S.; Kassinos, D.; Belgiorno, V.; Guida, M. Fate of pharmaceuticals in contaminated urban wastewater effluent under ultrasonic irradiation. *Water Res.* **2009**, *43*, 4019–4027. [CrossRef] [PubMed]
47. Chu, W.; Wong, C. The photocatalytic degradation of dicamba in $TiO_2$ suspensions with the help of hydrogen peroxide by different near UV irradiations. *Water Res.* **2004**, *38*, 1037–1043. [CrossRef] [PubMed]
48. Salari, D.; Daneshvar, N.; Aghazadeh, F.; Khataee, A. Application of artificial neural networks for modeling of the treatment of wastewater contaminated with methyl tert-butyl ether (MTBE) by $UV/H_2O_2$ process. *J. Hazard. Mater.* **2005**, *125*, 205–210. [CrossRef]
49. Kumar, U.; Kuntail, J.; Kumar, A.; Prakash, R.; Pai, M.R.; Sinha, I. In-situ $H_2O_2$ production for tetracycline degradation on $Ag/s\text{-}(Co_3O_4/NiFe_2O_4)$ visible light magnetically recyclable photocatalyst. *Appl. Surf. Sci.* **2022**, *589*, 153013. [CrossRef]
50. Shi, Y.; Li, J.; Wan, D.; Huang, J.; Liu, Y. Peroxymonosulfate-enhanced photocatalysis by carbonyl-modified g-C3N4 for effective degradation of the tetracycline hydrochloride. *Sci. Total. Environ.* **2020**, *749*, 142313. [CrossRef]
51. Fan, G.; Zheng, X.; Luo, J.; Peng, H.; Lin, H.; Bao, M.; Hong, L.; Zhou, J. Rapid synthesis of Ag/AgCl@ZIF-8 as a highly efficient photocatalyst for degradation of acetaminophen under visible light. *Chem. Eng. J.* **2018**, *351*, 782–790. [CrossRef]
52. Das, S.; Ahn, Y.-H. Synthesis and application of CdS nanorods for LED-based photocatalytic degradation of tetracycline antibiotic. *Chemosphere* **2022**, *291*, 132870. [CrossRef]
53. Mehrvar, M.; Anderson, W.A.; Moo-Young, M. Photocatalytic degradation of aqueous organic solvents in the presence of hydroxyl radical scavengers. *Int. J. Photoenergy* **2002**, *3*, 187–191. [CrossRef]
54. Kakavandi, B.; Takdastan, A.; Jaafarzadeh, N.; Azizi, M.; Mirzaei, A.; Azari, A. Application of $Fe_3O_4$@C catalyzing heterogeneous UV-Fenton system for tetracycline removal with a focus on optimization by a response surface method. *J. Photochem. Photobiol. A Chem.* **2015**, *314*, 178–188. [CrossRef]
55. Xu, P.; Ding, C.; Li, Z.; Yu, R.; Cui, H.; Gao, S. Photocatalytic degradation of air pollutant by modified nano titanium oxide ($TiO_2$)in a fluidized bed photoreactor: Optimizing and kinetic modeling. *Chemosphere* **2023**, *319*, 137995. [CrossRef] [PubMed]
56. Foroutan, R.; Peighambardoust, S.J.; Amarzadeh, M.; Korri, A.K.; Peighambardoust, N.S.; Ahmad, A.; Ramavandi, B. Nickel ions abatement from aqueous solutions and shipbuilding industry wastewater using ZIF-8-chicken beak hydroxyapatite. *J. Mol. Liq.* **2022**, *356*, 119003. [CrossRef]
57. López-Peñalver, J.J.; Sánchez-Polo, M.; Gómez-Pacheco, C.V.; Rivera-Utrilla, J. Photodegradation of tetracyclines in aqueous solution by using UV and $UV/H_2O_2$ oxidation processes. *J. Chem. Technol. Biotechnol.* **2010**, *85*, 1325–1333. [CrossRef]
58. Nagamine, M.; Osial, M.; Jackowska, K.; Krysinski, P.; Widera-Kalinowska, J. Tetracycline Photocatalytic Degradation under CdS Treatment. *J. Mar. Sci. Eng.* **2020**, *8*, 483. [CrossRef]
59. Amarzadeh, M.; Salehizadeh, S.; Damavandi, S.; Mubarak, N.M.; Ghahrchi, M.; Ramavandi, B.; Shahamat, Y.D.; Nasseh, N. Statistical modeling optimization for antibiotics decomposition by ultrasound/electro-Fenton integrated process: Non-carcinogenic risk assessment of drinking water. *J. Environ. Manag.* **2022**, *324*, 116333. [CrossRef]
60. Liang, Y.; Li, J.; Xue, Y.; Tan, T.; Jiang, Z.; He, Y.; Shangguan, W.; Yang, J.; Pan, Y. Benzene decomposition by non-thermal plasma: A detailed mechanism study by synchrotron radiation photoionization mass spectrometry and theoretical calculations. *J. Hazard. Mater.* **2021**, *420*, 126584. [CrossRef]
61. Yaghoot-Nezhad, A.; Wacławek, S.; Madihi-Bidgoli, S.; Hassani, A.; Lin, K.-Y.A.; Ghanbari, F. Heterogeneous photocatalytic activation of electrogenerated chlorine for the production of reactive oxygen and chlorine species: A new approach for Bisphenol A degradation in saline wastewater. *J. Hazard. Mater.* **2023**, *445*, 130626. [CrossRef] [PubMed]
62. Al-Musawi, T.J.; Moghaddam, N.S.M.; Rahimi, S.M.; Amarzadeh, M.; Nasseh, N. Efficient photocatalytic degradation of metronidazole in wastewater under simulated sunlight using surfactant- and CuS-activated zeolite nanoparticles. *J. Environ. Manag.* **2022**, *319*, 115697. [CrossRef]
63. Arghavan, F.S.; Al-Musawi, T.J.; Allahyari, E.; Moslehi, M.H.; Nasseh, N.; Panahi, A.H. Complete degradation of tamoxifen using $FeNi_3$@$SiO_2$@ZnO as a photocatalyst with UV light irradiation: A study on the degradation process and sensitivity analysis using ANN tool. *Mater. Sci. Semicond. Process.* **2021**, *128*, 105725. [CrossRef]

64. Wang, J.; Xia, Y.; Zhao, H.; Wang, G.; Xiang, L.; Xu, J.; Komarneni, S. Oxygen defects-mediated Z-scheme charge separation in g-C3N4/ZnO photocatalysts for enhanced visible-light degradation of 4-chlorophenol and hydrogen evolution. *Appl. Catal. B Environ.* **2017**, *206*, 406–416. [CrossRef]
65. Wang, J.; Zhang, Q.; Deng, F.; Luo, X.; Dionysiou, D.D. Rapid toxicity elimination of organic pollutants by the photocatalysis of environment-friendly and magnetically recoverable step-scheme SnFe2O4/ZnFe2O4 nano-heterojunctions. *Chem. Eng. J.* **2020**, *379*, 122264. [CrossRef]

**Disclaimer/Publisher's Note:** The statements, opinions and data contained in all publications are solely those of the individual author(s) and contributor(s) and not of MDPI and/or the editor(s). MDPI and/or the editor(s) disclaim responsibility for any injury to people or property resulting from any ideas, methods, instructions or products referred to in the content.